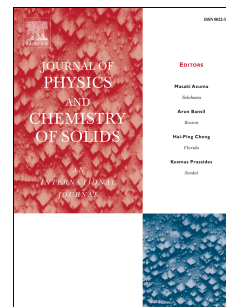


Accepted Manuscript

Electrophysical properties of hydroxylated endohedral metallofullerene with gadolinium

Alexander I. Dudnik, Natalia G. Vnukova, Nikolay A. Drokin, Vitaliy S. Bondarev, Nikolay P. Shestakov, Yevgeniy V. Tomashevich, Grigory N. Churilov



PII: S0022-3697(19)30547-5

DOI: <https://doi.org/10.1016/j.jpcs.2019.109094>

Article Number: 109094

Reference: PCS 109094

To appear in: *Journal of Physics and Chemistry of Solids*

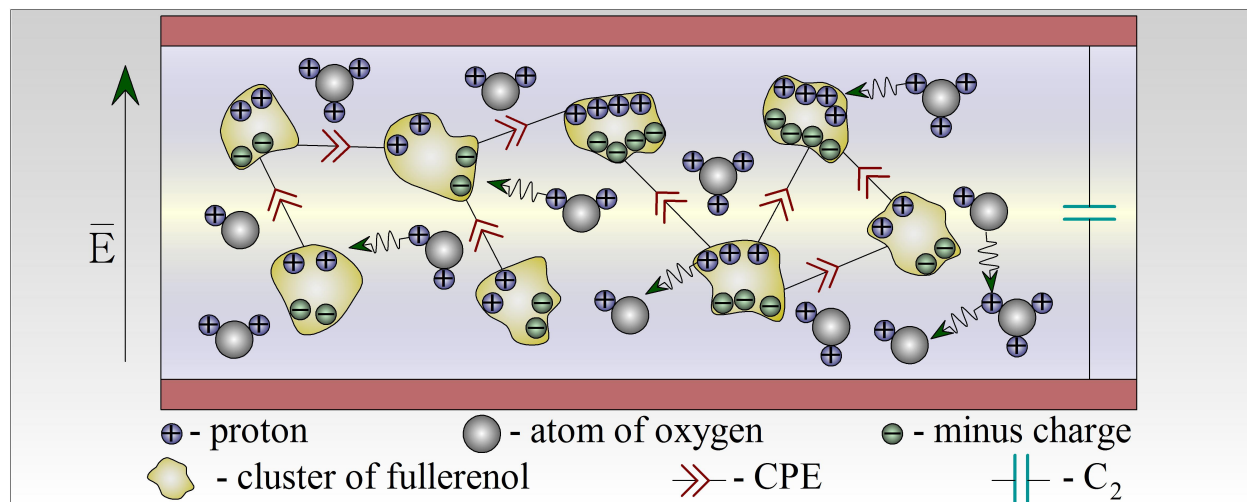
Received Date: 11 March 2019

Revised Date: 27 June 2019

Accepted Date: 10 July 2019

Please cite this article as: A.I. Dudnik, N.G. Vnukova, N.A. Drokin, V.S. Bondarev, N.P. Shestakov, Y.V. Tomashevich, G.N. Churilov, Electrophysical properties of hydroxylated endohedral metallofullerene with gadolinium, *Journal of Physics and Chemistry of Solids* (2019), doi: <https://doi.org/10.1016/j.jpcs.2019.109094>.

This is a PDF file of an unedited manuscript that has been accepted for publication. As a service to our customers we are providing this early version of the manuscript. The manuscript will undergo copyediting, typesetting, and review of the resulting proof before it is published in its final form. Please note that during the production process errors may be discovered which could affect the content, and all legal disclaimers that apply to the journal pertain.



ACCEPTED MANUSCRIPT
**ELECTROPHYSICAL PROPERTIES OF HYDROXYLATED ENDOHEDRAL
METALLOFULLERENE WITH GADOLINIUM**

Alexander I. Dudnik^{1,2}, Natalia G. Vnukova^{1,2}, Nikolay A. Drokin¹,
Vitaliy S. Bondarev^{1,2}, Nikolay P. Shestakov^{1,2}, Yevgeniy V. Tomashevich³, Grigory N. Churilov^{1,2}

¹ Kirensky Institute of Physics, Federal Research Center KSC SB RAS

² Siberian Federal University, Krasnoyarsk, Russia.

³ Institute of Chemistry and Chemical Technology SB RAS, Krasnoyarsk, Russia

The paper presents the results of experimental measurements of constitutive and electrophysical properties in hydroxylated endohedral metallofullerene with gadolinium sample. We extracted endohedral metallofullerene from carbon condensate, synthesized in high-frequency arc discharge plasma. Later hydroxyl groups were added. Via methods of infrared and x-ray photoelectronic spectroscopy, it was established that the molecules of hydroxylated endohedral metallofullerene have the $Gd@C_{82}O_x(OH)_y$, $x+y=(40-42)$ composition. The method of measuring the electrical impedance in the frequency range from 100 Hz to 100 MHz shows that the resulting hydroxylated fullerene is an ion conductor. The measured frequency dependences of the dielectric permittivity and conductivity of hydroxylated fullerene are explained based on the assumption of an inhomogeneous distribution of electric charges in the material volume. Dielectric-hysteresis loops in the frequency range of 25 Hz – 1 MHz and temperature range of 80 - 300 K, and volt-ampere characteristics were measured. The obtained results imply the appearance of residual polarization induced by the electric field in hydroxylated fullerene. However, the constant dipole moment is absent.

Keywords: endohedral metallofullerene, fullerenol, impedance, dielectric permittivity, ionic and proton conductivity, dielectric hysteresis, polarizability.

Introduction

The structure of the endohedral metallofullerene (EMF) molecule differs significantly from the structure of conventional fullerene molecules. Inside the EMF molecule, there is a metal ion, valence electrons of which are accepted by the π -system of the carbon cage [1]. Depending on the fullerene size and type and number of encapsulated atoms, endohedral metallofullerenes can be in a form of metal, semiconductors with a small band gap, or dielectrics. In particular, the injection of rare-earth element ions can be expected to produce a dipole or magnetic moment. At the moment, EMF with magnetic moment has been synthesized and studied [2-4].

Since the metal ion in the EMF molecule is displaced from the center of the cage [5], the electric dipole moment occurs in this molecule under certain conditions. This was detected, for example, in $La@C_{82}$ films [6]. This fullerene has a sufficiently high value of dielectric permittivity ($\epsilon = 10 - 20$ at frequency $f = 1$ MHz). The above two features of EMF molecules are manifested in their ability to operate as a field effect transistor [7], as an organic solar cell [8], as part of a memory device in molecular electronics [9]. Another possible use is as an additive to various materials to improve their thermoelectric properties [10]. Such materials are used in power generation and production of heat insulation in solid-state memory devices [11, 12].

The dipole moment can also occur in hydroxylated fullerenes (fullerenols), in which O and OH groups are attached to the cage of the main molecule. The polarizability of these fullerenols will depend on the number of attached functional O and OH groups. And their mutual arrangement on the

frame of the main molecule affects their chemical and electrophysical properties [13]. EMF with OH and other more complex groups attached to the framework are promising for use in biomedicine: in magnetic resonance imaging [14] and as an anti-cancer agent [15]. It is known that fullerenols based on C_{60} and C_{70} possess ionic conductivity, which depends on the number of OH groups [16], therefore, the appearance of ionic conductivity in hydroxylated $Gd@C_{82}$ is also quite expected. The introduction of fullerenes and fullerenols tend to improve the electrical and temperature characteristics of polymer ionic conductors, such as Nafion® [17, 18, 19], which are widely used in fuel cells. The electron affinity of $Gd@C_{82}$ is greater than that of C_{60} (3.3 and 2.7 ± 0.1 eV, respectively) [20], so it can add more radicals. In addition, the presence of a dipole moment in EMF can be used to change the dielectric constant of materials. So far, detailed studies on the EMF electrophysical properties and fullerenols based on them in the form of powders or films have not yet been conducted.

This paper is devoted to the development of technology for the production and measurement of electrical and ferroelectric properties of hydroxylated fullerene $Gd@C_{82}$. This fullerene was synthesized and isolated in an amount sufficient for experiments. The electrophysical properties of the obtained fullerenol were investigated by measuring the electrical impedance in the frequency range of 10^2 – 10^8 Hz. We also analyzed experimentally measured volt-ampere characteristics and dielectric-hysteresis loops in the frequency range of 25 Hz–1 MHz and temperatures of 80–300 K.

1. Synthesis and physical properties of hydroxylated $Gd@C_{82}$

Carbon condensate, containing $Gd@C_{82}$, was synthesized in the plasma of high-frequency arc discharge by spraying graphite electrodes with axial holes of 3 mm in diameter, containing a mixture of Gd_2O_3 powder and graphite in a ratio of 1:1 by weight, [21]. We extracted the fullerene mixture out of the obtained carbon condensate using carbon disulfide in the Soxhlet extractor. Following the method based on the use of Lewis acids $TiCl_4$, from the obtained solution we extracted the mixture $Gd@C_{82}$ and higher fullerenes [22]. Then the solvent evaporated and the resulting solid fraction was dissolved in toluene. Fullerene $Gd@C_{82}$ was extracted from the solution via high-performance liquid chromatography using Agilent Technologies 1200 Series chromatograph (the column Cosmosil Buckyprep M; toluene stream 5 ml/min). O and OH groups were attached to the isolated EMF by treatment with HNO_3 acid and further washing in distilled water [23].

On the mass-spectrometer MALDI-TOF Bruker BIFLEX TM III, we have obtained the mass spectrum of fullerene $Gd@C_{82}$, presented in Fig. 1.

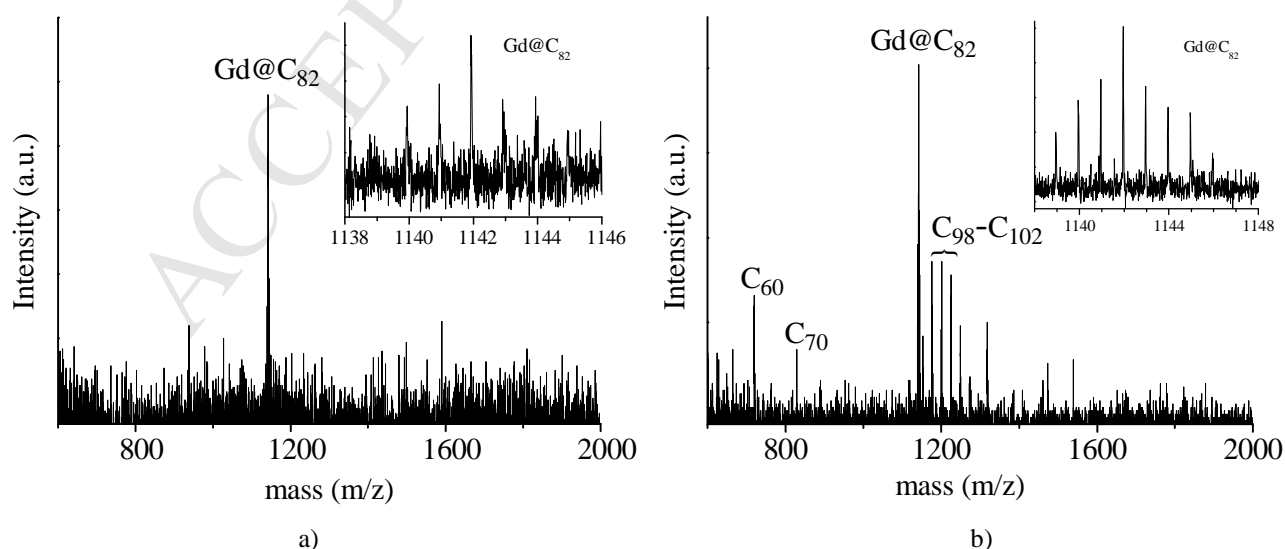


Fig. 1. Mass spectrum of the chromatographic fraction with $Gd@C_{82}$: a - positive mode; b - negative mode

As shown, in the mass spectrum only the main fraction Gd@C_{82} is present, well isolated from broadband noise. Hydroxylated fullerene Gd@C_{82} was also studied via IR spectroscopy using Fourier spectrometer VERTEX 70 by Bruker in the matrix of KBr. In the infrared fullereneol transmission spectrum (Fig.2) there is broadband at OH groups (dotted line $\nu_{\text{O-H}}$), against which the peak from bond C-H (dotted line $\nu_{\text{C-H}}$) are well distinguished. According to the sources [3, 24, 25], absorption band from the bonds C-C (1554 cm^{-1}), C=C (1621 cm^{-1}), C=O (1703 cm^{-1}), C-O ($1050\text{-}1150 \text{ cm}^{-1}$) were identified.

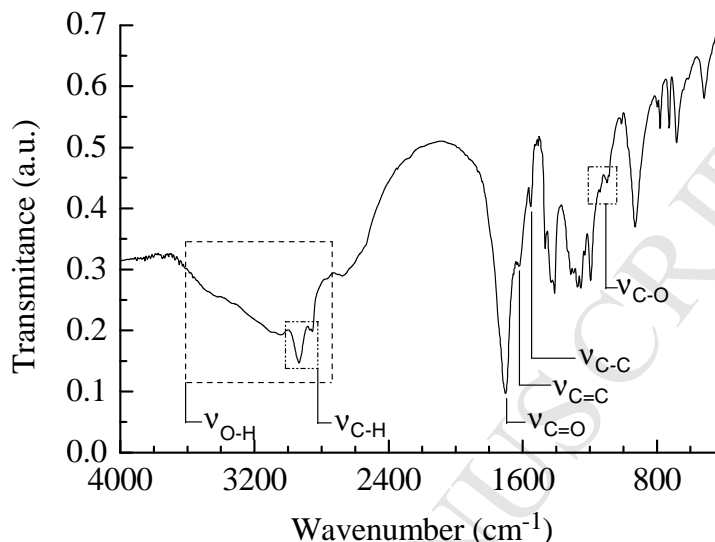


Fig. 2. Infrared transmission spectrum $\text{Gd@C}_{82}\text{O}_x(\text{OH})_y$ in the matrix of KBr

The study of fullereneol was also carried out by x-ray photoelectronic spectroscopy (XPS) via the device UNI-SPECS spectrometer, SPECS GmbH. Fig. 3 shows the carbon C1s spectrum lines (solid line), and where after Lorentz decomposition three lines were distinguished (dotted line). The line with the maximum at 284.7 eV corresponds to the bond between the carbon atoms in the C_{82} molecule. The line with the maximum at 286.2 eV corresponds to the hydroxyl bond C-OH, and the peak is at 289 eV - carbonyl bond C=O.

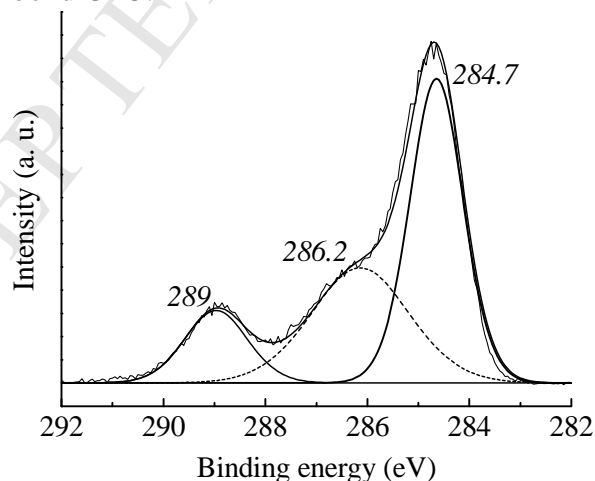


Fig. 3. XPS C1s line

Thus, in the process of hydroxylation, both oxygen (C=O) and hydroxyl groups (C-OH) attach to the fullerene molecule cage. The number of these functional groups was calculated on the basis of XPS, based on the proportion of carbon atoms chemically bonded with oxygen. Given that the number of OH groups attached to the fullerene must be even [26], the composition of the product, determined on the basis of the XPS analysis, can be presented as $\text{Gd@C}_{82}\text{O}_x(\text{OH})_y$, where $x=10\text{-}12$ and $y=30\text{-}32$, $x+y=40\text{-}42$.

2. Sample preparation and measurement

Prior to measuring the electrical characteristics, the hydroxylated EMF was dried with a moisture absorber P_2O_5 at a temperature of $23\text{ }^{\circ}\text{C}$ for 2 weeks. Via the method of gravimetric and differential thermal analysis (spectrometer STA 449 C Jupiter from Netzsch) of hydroxylated fullerene $Gd@C_{82}$ in an argon atmosphere, it was determined that the substance contains 1.4 wt. % water.

For electrophysical measurements the test sample was placed in a special measuring cell (Fig. 4), serving as a capacitor. The cell consists of two metalized textolite plates (1) with etched electrodes (2). The narrow part of the electrodes was used to connect the cell to the measuring instruments. Between the wide parts of $5\times 5\text{ mm}$ in size we placed fullerenol. Between the plates, we placed a 0.1 mm thick fluoroplastic layer (3) with a cutout that was aligned with the electrodes during assembly. The layer recorded the thickness of the investigated fullerene sample. A fullerenol sample (4) in a pasty state was placed in the gap of the fluoroplastic laying and clamped between the electrodes. Textolite plates were pressed with the specialized holder.

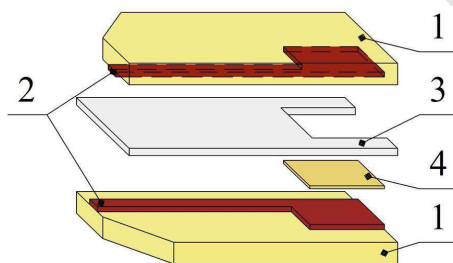


Fig. 4. Cell for measuring the conductivity of fullerenol:
1-fiberglass; 2-copper electrode; 3-fluoroplast; 4-investigated sample

3. Study of electrophysical characteristics by impedance spectroscopy method

Impedance measurements were performed using the Network Analyzer E5061B Agilent Technologies. The measurements were directly focused on the frequency dependence of the scalar impedance $|Z|$ and phase angle φ between the current and voltage. Then we calculated the real and imaginary impedance components (Z' , Z''), dielectric permittivity (ϵ' , ϵ''), conductivity (σ' , σ'') and dielectric loss $\text{tg}\delta$ [27].

Fig. 5 shows the dependence of the real dielectric part of the permittivity ϵ' and the dielectric loss $\text{tg}\delta$ of the sample from the electric field frequency.

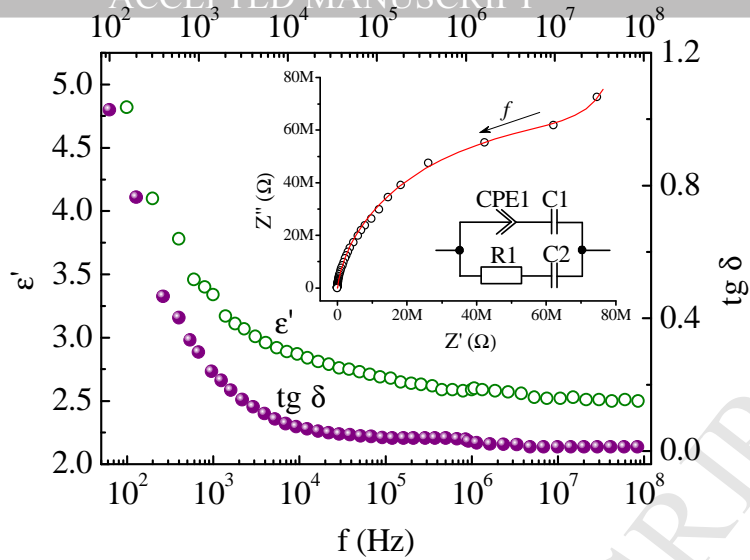


Fig. 5. Dependence ϵ' and $\text{tg}\delta$ sample on frequency. Inset shows the hodograph and its approximation based on the equivalent circuit

As can be seen, the value of the fulleranol dielectric constant (2.5) at frequencies of $10^7 - 10^8$ Hz is nearly indistinguishable from ϵ' for fullerene C_{60} ($\epsilon' \approx 2.6$), and $\text{tg}\delta = 0.018$. However, with decreasing of frequency up to 100 Hz ϵ' increase to the value of 4.8, which is accompanied by the increase of the dielectric loss $\text{tg}\delta \geq 1$. To better understand the processes of dielectric polarization and movement of electric charges happening in the studied substance, we included an inset of impedance hodograph in fig. 5. The impedance hodograph was constructed in Nyquist coordinates as the frequency dependence of the imaginary impedance part $Z''(f)$ on real part $Z'(f)$ [28, 29]. Each point of the hodograph corresponds to a certain frequency. The countdown begins at the right side of the hodograph semicircle. The construction of the impedance hodograph largely contributes to the search for a suitable equivalent circuit, the impedance of which is to approximate the experimentally measured frequency dependences of the impedance module, dielectric permittivity and the loss tangent of the sample. The most suitable equivalent circuit is shown in the same fig. 5 and consists of two parallel circuits. The lower circuit contains resistance $R_1 = 1.3 \cdot 10^8 \Omega$ and capacity $C_2 = 2.5 \cdot 10^{-11} F$, which are connected in series. This chain is used to approximate the initial arc of the hodograph semicircle. The upper circuit contains a specific frequency-dependent element CPE_1 [30] and a capacitor C_1 . Element CPE_1 has both real and imaginary parts of the impedance. It can be compared to the conductivity and frequency-dependent capacity, which occurs due to the accumulation of electric charges near the electrodes or at the boundaries of inhomogeneous areas with different moisture content in fulleranol. The electric charge in the volume of fulleranol can be transmitted with the participation of H^+ , H_3O^+ and OH^- ions. Conductivity is carried out by the relay mechanism of charge transferring through the extended hydrogen-bond networks between water molecules present in the structure of fulleranol. This spatial redistribution of charges partially shields the external electric field. This is the main reason for the increase in the real and imaginary components of the dielectric permittivity and dielectric loss in the low-frequency region.

Fig. 6 shows the frequency dependences of the real σ' and imaginary σ'' components of the specific conductivity. At low frequencies near 10^2 Hz, they do not exceed 10^{-8} S/m and rise with increasing frequency.

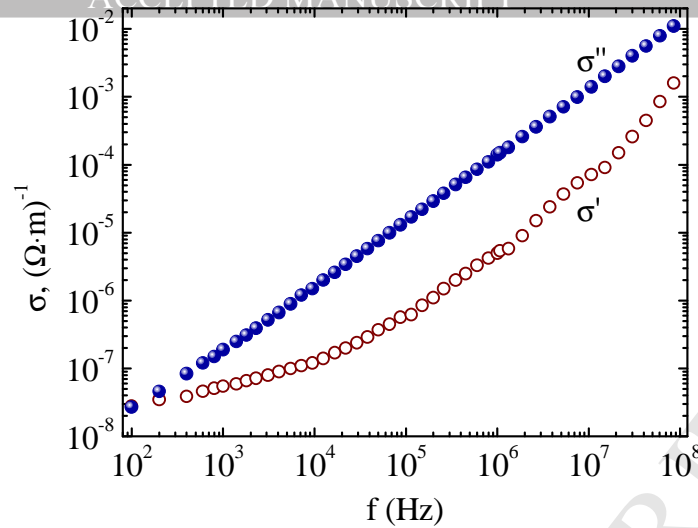


Fig. 6. Specific conductivity of the sample depending on the frequency

The imaginary conductivity component in logarithmic coordinates increases linearly as $\sigma''(f) = 2\pi \cdot f \cdot C_{\text{eff}}(f)$. The increase of the real conductivity component occurs in proportion to the circular frequency with a fractional exponent and can be approximated by the following equation:

$$\sigma'(\omega) = 2.6 \cdot 10^{-8} + 3 \cdot 10^{-12} \cdot \omega^{0.94} \quad (1)$$

Such conductivity dependence is realized in many materials having electron or ion conductivity of hopping type. The directed motion of charge carriers, in this case, occurs by their jump between ions with different valence [31]. However, the index close to one suggests a high charge velocity, which is more typical for proton conductivity. The mechanism of generation and transferring of electric charges in $\text{Gd@C}_{82}\text{O}_x(\text{OH})_y$ is not clear yet. However, it is undoubtedly associated with the presence of physically bound water in the composition of fulleranol, which persists even after prolonged drying via the mentioned method.

4. The dynamic process of fulleranol polarization

In order to clarify in detail the mechanisms of dielectric polarization of this fulleranol, we measured the temperature dependence of the dielectric permittivity as well as the dielectric loss tangent. We also studied the dynamic characteristics of the dielectric hysteresis loops in the temperature range of 80-300 K. The dependence measurements based on $\epsilon'(T)$ were performed using the RLC meter E7-20 at frequencies of 25 Hz and 1 MHz in the adiabatic conditions in the heating mode at a speed in the range of 0.5-2 K/min. The electric capacity of the fulleranol sample and the dielectric loss tangent were measured. The calculation of the real dielectric permittivity constant of the $\epsilon'(T)$ was performed according to the well-known formula for the plate capacitor. The physical dimensions of the measuring cell were taken into account. The measurement results are shown in Fig. 7.

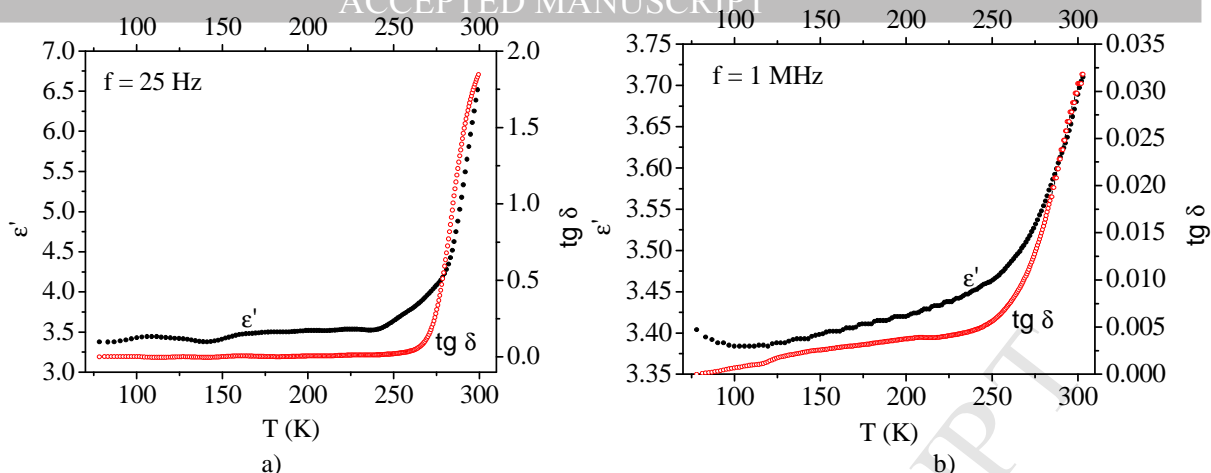


Fig. 7. Values $\epsilon'(T)$ and $\text{tg}\delta(T)$ for the fullerol sample at the frequencies 25 Hz (a) and 1 MHz (b)

As can be seen, with increasing temperature from 77 K to 250 K, at 25 Hz and 1 MHz, dielectric permittivity and dielectric loss in the beginning, almost do not change, remaining at $\epsilon' \approx 3.4$ – 3.5 and $\text{tg}\delta \approx 0.001$ – 0.003 . However, with further temperature increase the level of dielectric permittivity and dielectric loss increases. Probably, when increasing temperature, crystals of physically bound water gradually melt. The processes of movement and accumulation of electric charges on the electrodes and between the individual structural regions of fullerol become more intense. This increases the polarizability of fullerol and leads to an increase in the dielectric permittivity and dielectric loss value. It should be noted that the dielectric permittivity value of fullerol at low temperatures ~ 77 – 100 K ($\epsilon' \approx 3.4$ – 3.5) is higher than that of fullerene C_{60} (2.6). This value is lower than that of C_{70} (4.6) [32]. Perhaps this is connected to the appearance of additional polarization of the fullerol molecule itself due to the presence of the Gd^{3+} ion inside of it. Due to the presence of OH groups, proton-type conductivity can occur even at such low temperatures. Dipole moments of hydroxyl groups partially compensate for the dipole moment of the EMF molecule, making its total value less than 4.6.

Dynamic processes of fullerol polarization were investigated by analyzing the dielectric-hysteresis loops, obtained at specified temperatures at a setup Easy Check 300. The measuring electrical circuit in the setup is a resistive-capacitive divider consisting of a capacitive cell with a sample (Fig. 4) and series resistance included. The optimal value of this resistance was chosen based on the value of the current passing through the sample. Triangular waveform voltage was applied to the measuring circuit with a maximum electric field strength of 20 kV/cm and a frequency of 0.1 Hz (voltage rise rate of 8 kV/s). This low frequency was used to identify any possible slow processes of motion, accumulation, and relaxation of mobile electric charges, that determine the value of dielectric polarization and reach-through conductivity.

In the course of measurements, the device recorded the dependence of the current passing through the sample $I(t)$ and the voltage applied to the divider $U(t)$. The polarization value P (C/cm^2) was determined by the following formula:

$$P = \frac{1}{S} \sum_{i=0}^n I_i \cdot t_i \quad (2)$$

where S is the contact area of the measuring cell. The measurements were carried out at fixed temperatures in a high vacuum 10^{-5} Pa. To implement the adiabatic conditions of the experiment, we used a calorimeter in the continuous heating mode at a rate of 0.5 K/min. The sample temperature was controlled by a platinum thermometer. The results of measurements of dielectric-hysteresis loops are shown in Fig. 8.

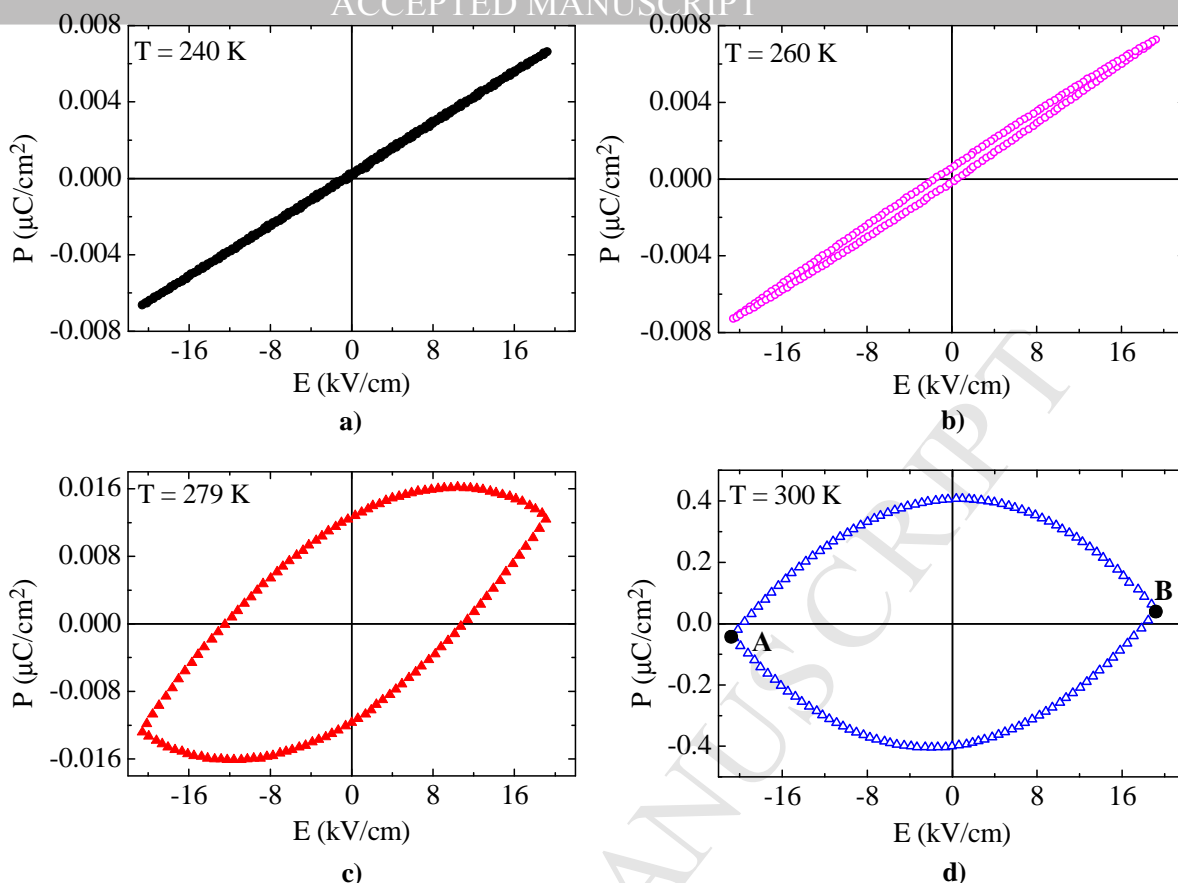


Fig. 8. Dielectric-hysteresis loops at different temperatures

As seen in Fig. 8a, at a temperature of 240 K the polarization of the sample linearly depends on the field. This is typical for many dielectrics with electronic type polarization and, in particular, for conventional fullerenes. However, with a small increase in temperature to 260 K, the opening of the dielectric-hysteresis loop occurs (Fig. 8b). And at zero values of electric field, there is a residual polarization of $3.3 \cdot 10^{-4} \mu\text{C}/\text{cm}^2$. This residual polarization arises either because of the presence of the gadolinium ion inside the fullerene molecule or because of the hydroxyl groups present. Hydroxyl groups can initiate intramolecular proton conductivity and non-equilibrium redistribution of electric charges even at these relatively low temperatures.

With the temperature increase up to 279 K (Fig. 8c), there is an almost double increase in the polarization of fullerene and deformation of the hysteresis loop. This is connected to the appearance of reach-through conductivity. Due to the active component of the reach-through electric current, this results in an additional voltage drop in a removable resistance of the resistive-capacitive divider. The appearance of reach-through conductivity leads to an *apparent* increase in the modulus of the polarization vector P . In addition, big electrical circuit time constant ($\tau=R \cdot C$) leads to delaying of the sample recharging and broadening of the hysteresis loop. With further increase in temperature, as seen in Fig. 8d, the effect of the reach-through conductivity is enhanced (the hysteresis loop is distorted). At the points marked with the letters A and B polarization cannot be calculated but is mainly determined by the active component of the current.

Since the sample has reach-through conductivity, it is very difficult to determine whether there is an internal residual and possibly spontaneous polarization along with the usual surface polarization. In this paper, for a more detailed study of polarization, the method PUND (Positive Up Negative Down) was used. This allowed distinguishing spontaneous polarization from electric charges accumulated on various defects [33].

The measurement results are presented in the form of the dependence of the switching current on the electric field strength. This was done for a visual representation of the difference between the switching currents areas when two impulses of the same direction are applied. The presence of

significant current extremum on the dependence $I(E)$ will indicate the presence of spontaneous polarization in the sample. The results of ferroelectric switching measurements via the PUND method are shown in Fig. 9.

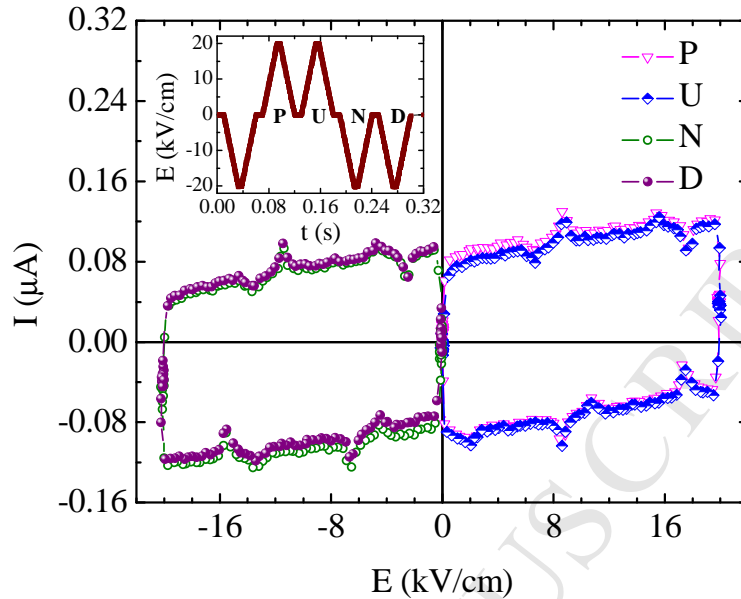


Fig. 9. Ferroelectric switching measurement of the sample via the PUND method

It is clearly seen that for the studied fulleranol, the dependences $I(E)$ for switching currents, when applying voltage pulses in one direction, almost coincide. Therefore, residual polarization in fulleranol is rather insignificant (the value is given above). There is also no spontaneous polarization.

Fig. 10 shows volt-ampere characteristics (VAC) measured at a temperature of 300 K with a linear voltage scan at different frequencies. VAC measurements were performed using a resistive-capacitive divider similar to that used for hysteresis loop measurements. The dependence of the phase angle between the current and voltage of the electric field period T is shown in Fig. 11. The phase angle between current and voltage was defined as the arcsine of the distance ratio between the points of VAC intersection and the abscissa axis to the total width of the VAC along the same axis.

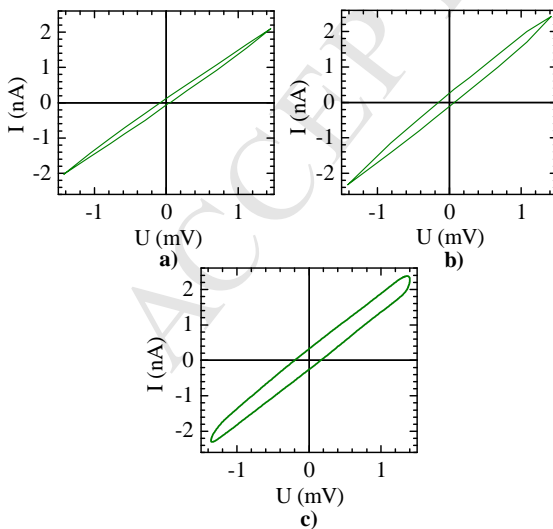


Fig. 10. Volt-ampere characteristics of $\text{Gd}@C_{82}O_x(OH)_y$ at frequency: a – 0.01 Hz; b – 0.2 Hz; c – 0.8 Hz

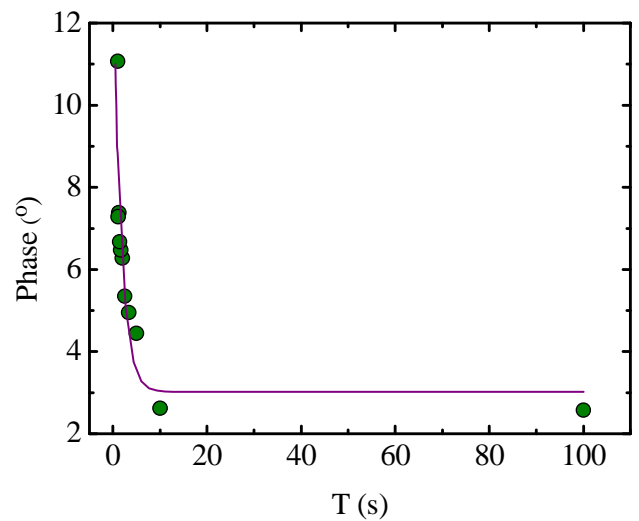


Fig. 11. Exponential dependence of the phase angle between current and sample voltage on the voltage period

As seen in Fig. 10a, at a low electric field scan frequency, the rise and fall of the current through the sample occurs with a small phase lag $\phi = 2.52^\circ$ from the voltage. It is seen (in Fig. 10 and

11) that with an increase in the scan frequency of the electric field the phase angle increases. At $f = 0.8$ Hz (Fig. 10c) it reaches a value of 7.4° . An increase in the phase angle (i.e., the time between the current and voltage increases) indicates an increase in reach-through conduction. At frequencies less than 0.1 Hz, the reach-through conductivity is almost unchanged.

5. Discussion of the results

The analysis of the dependences $\sigma'(f)$ and $\sigma''(f)$ shows that the charge carriers in the fullereneol $\text{Gd@C}_{82}\text{O}_x(\text{OH})_y$ ($x=10-12$ и $y=30-32$, $x+y=40-42$) are protons. The protons arise from the dissociation of water molecules or as a result of the separation of the fullereneol molecules from the OH groups [34]. Water is in between the molecules of fullereneol and the protons transfer between them through the water bridges. It is possible that protons when getting into the environment of water molecules, form H_3O^+ hydroxonium ions, which transfer protons among fullereneol molecules. This explains the dependence $\varepsilon'(T)$. At a frequency of 25 Hz in the temperature range 300-250 K water dipole moment, located among the fullereneol molecules, makes a major contribution to the value ε' . As the temperature decreases, the water turns into ice and ε' almost does not change, since the proper dipole moments of fullereneol molecules are extremely small. $\text{tg}\delta$ decreases by two orders of magnitude, which indicates a change in the mechanism of charge transfer. At temperatures below 250 K protons are no longer able to move among fullereneol molecules on water bridges. This happens due to the fact that the conductivity of ice is negligible, and protons move jumping on the relay mechanism. At a frequency of 1 MHz, up to a temperature of 100 K, it is not possible to distinguish the effect dipole moments of water molecules and fullereneol have on ε' and $\text{tg}\delta$. This requires a further decrease in temperature and possibly an increase in frequency.

The experimental data obtained from the dielectric-hysteresis loops are in good agreement with the dielectric data. It confirms the nonlinearity of the dielectric properties of the substance under study. As the temperature increases, the residual polarization increases, and at a temperature of 300 K, the shape of the hysteresis loop approaches the shape of the rugby ball. This shape is due to the presence of a large reach-through conductivity in fullereneol, which does not allow it to reach the state of ferroelectric saturation.

In our case, the hodograph branch is not clearly defined, therefore we can speak only about the order of the magnitude of the proton conductivity, which is 10^{-10} S/cm. As shown in [35], proton conductivity depends on the number of OH groups attached, but with their increase from 12 to 24 proton conductivity decreases by several orders of magnitude. Therefore, the low proton conductivity of $\text{Gd@C}_{82}\text{O}_x(\text{OH})_y$ can be associated with oxygen atoms attached to the EMF frame and a large number of OH groups.

Conclusion

The measurements showed that fullereneol $\text{Gd@C}_{82}\text{O}_x(\text{OH})_y$ ($x+y=40-42$) is a poor proton conductor with the ionic conductivity of 10^{-10} S/cm. At 10^8 Hz, the real dielectric constant and the dielectric loss are 2.6 and 0.018, respectively. It is shown, based on the dielectric hysteresis loop forms and PUND measurements, that there is no spontaneous and residual polarization at temperatures above 260 K in fullereneol. At temperatures near 260 K and below, there is a residual polarization of $3.3 \cdot 10^{-4}$ $\mu\text{C}/\text{cm}^2$ in fullereneol. The presence of residual polarization (and, as a consequence, ε' of 3.5 in value at the same temperatures) is explained by the existence of the dipole moment in EMF molecules, as well as the dipole moment formed by hydroxyl and oxygen groups.

The equipment was provided by the Collective Use Center — Kirensky Institute of Physics, Federal Research Center KSC Siberian Branch Russian Academy of Sciences.

The reported study was funded by RFBR according to the research project № 18-29-19003.

References

1. H. Shinohara, Endohedral metallofullerenes, Report of progress in physics 63 (2000) 843-892.
2. J. Zhang, Y. Ye, Y. Chen, C. Pregot, T. Li, S. Balasubramaniam, D. B. Hobart, Y. Zhang, S. Wi, R. M. Davis, L. A. Madsen, J. R. Morris, S. M. LaConte, G. T. Yee, H. C. Dorn, Gd₃N@C₈₄(OH)_x: A new egg-shaped metallofullerene magnetic resonance imaging contrast agent, J. Am. Chem. Soc. 136 (2014) 2630-2636, DOI: 10.1021/ja412254k.
3. J. Li, T. Wang, Y. Feng, Y. Zhang, M. Zhen, C. Shu, L. Jiang, Y. Wang, C. Wang, A water-soluble gadolinium metallofullerene: facile preparation, magnetic properties and magnetic resonance imaging application, Dalton Transactions 45 (2016) 8696-8699, DOI: 10.1039/C6DT00223D
4. H. J. Huang, S. H. Yang, X. X. Zhang, Magnetic behavior of pure endohedral metallofullerene Ho@C₈₂: a comparison with Gd@C₈₂, J. Phys. Chem. B 103 (1999) 5928-5932.
5. K. Kobayashi, S. Nagase, Structures and electronic states of M@C₈₂ (M=Sc, Y, La and lanthanides), Chemical Physics Letters 282 (1998) 325-329.
6. C. J. Nuttall, Y. Hayashi, K. Yamazaki, T. Mitani, Y. Iwasa, Dipole dynamics in the endohedral metallofullerene La@C₈₂, Advanced materials 14 (2002) 293-296, DOI: 10.1002/1521-4095(20020219)14:4<293::AID-ADMA293>3.0.CO;2-I.
7. Shin-ichiro Kobayashi, S. Mori, S. Iida, H. Ando, T. Takenobu, Y. Taguchi, A. Fujiwara, A. Taninaka, H. Shinohara, and Y. Iwasa, Conductivity and field effect transistor of La₂@C₈₀ metallofullerene, Journal of the American chemical society 125(27) (2003) 8116-8117, DOI: 10.1021/ja034944a.
8. R. B. Ross, C. M. Cardona, D. M. Guldi, S. G. Sankaranarayanan, M. O. Reese, N. Kopidakis, J. Peet, B. Walker, G. C. Bazan, E. Van Keuren, B. C. Holloway and M. Drees, Endohedral fullerenes for organic photovoltaic devices, Nature materials 8 (2009) 208-212 DOI: 10.1038/NMAT2379.
9. D. Yue, R. Cui, X. Ruah, H. Huang, X. Guo, Z. Wang, X. Gao, S. Yang, J. Dong, F. Yi, B. Sun, A novel organic electrical memory device based on the metallofullerene-grafted polymer (Gd@C₈₂-PVK), Organic electronics 15(12) (2014) 3482-3486, DOI: 10.1016/j.orgel.2014.09.041.
10. T. Mondal, A. Tripathi, J. Zhang, T. Shripathi, H. Shinohara and A. Tiwari, Thermal conductivity of M@C₈₂ [M = Dy, Gd] thin films, The journal of physical chemistry C 121 (2017) 3642-3647, DOI: 10.1021/acs.jpcc.6b12577
11. K. Zhang, Y. Zhang, S. R. Wang, Enhancing thermoelectric properties of organic composites through hierarchical nanostructures, Scientific reports 3 (2013) 3448, DOI: 10.1038/srep03448.
12. K. F. Hsu, S. Loo, F. Guo, W. Chen, J. S. Dyck, C. Uher, T. Hogan, E. Polychroniadis, M. G. Kanatzidis, Cubic AgPb_mSbTe_{2+m}: bulk thermoelectric materials with high figure of merit, Science 303 (2004) 818-821.
13. J. Tang, G. M. Xing, F. Zhao, H. Yuan, Y. L. Zhao, Modulation of structural and electronic properties of fullerene and metallofullerenes by surface chemical modifications, J. Nanosci. Nanotechnol 7 (2007) 1085-1101.
14. H. Kato, Y. Kanazawa, M. Okumura, A. Taninaka, T. Yokawa, H. Shinohara, Lanthanoid endohedral metallofullerenols for MRI contrast agents, Journal of the American chemical society 125(14) (2003) 4391-4397, DOI: 10.1021/ja027555+.
15. P. P. Fatouros, F. D. Corwin, Z.-J. Chen, W. C. Broaddus, J. L. Tatum, B. Kettenmann, Z. Ge, H. W. Gibson, J. L. Russ, A. P. Leonard, J. C. Duchamp, H. C. Dorn, In vitro and in vivo imaging studies of a new endohedral metallofullerene nanoparticle, Radiology 240(3) (2006) 756-764, DOI: 10.1148/radiol.2403051341.
16. Z. Slanina, S.-L. Lee, L. Adamowicz, L.Y. Chiang, Structural computations of fullerols C₆₀(OH)_n, Proc. Electrochem. Soc. (Rec. Adv. Chem. Phys. Fullerenes Relat. Mater., vol. 3) 96 (1996) 987.

17. Tasaki K., DeSousa R., Wang H.B., Gasa J., Venkatesan A., Pugazhendhi P., Loutfy R.O. // *J. Membr. Sci.* 2006. Vol. 281. P. 570. DOI: 10.1016/j.memsci.2006.04.052.
18. Wang H., DeSousa R., Gasa J., Tasaki K., Stucky G., Joussetme B., Wudl F. // *J. Membr. Sci.* 2007. Vol. 289. P. 277. DOI: 10.1016/j.memsci.2006.12.008.
19. J-H. Jung S. Vadahanambi, Il-K. Oh Electro-active nano-composite actuator based on fullerene-reinforced Nafion. *Composites science and technology.* – 2010. – V. 70. – P. 584-592.
20. O. V. Boltalina, I. N. Ioffe, I. D. Sorokin, L. N. Sidorov, Electron affinity of some endohedral lanthanide fullerenes, *The journal of physical chemistry A*, 101(50) 1997 9561-9563, DOI: 10.1021/jp972643f.
21. G. N. Churilov, W. Kratschmer, I. V. Osipova, G. A. Glushenko, N. G. Vnukova, A. L. Kolonenko, A. I. Dudnik, Synthesis of fullerenes in a high-frequency arc plasma under elevated helium pressure, *Carbon* 62 (2013) 389-392, <http://dx.doi.org/10.1016/j.carbon.2013.06.022>
22. K. Akiyama, T. Hamano, Y. Nakanishi, E. Takeuchi, S. Noda, Z. Wang, S. Kubuki, and H. Shinohara, Non-HPLC rapid separation of metallofullerenes and empty cages with TiCl_4 Lewis acid, *Journal of the American Chemical Society* 134 (2012) 9762-9767, DOI: 10.1021/ja3030627.
23. L. Y. Chiang, J. W. Swirczewski, C. S. Hsu, S. K. Chowdhury, S. Cameron, and K. Creegan, Multi-hydroxy additions onto C_{60} fullerene molecules, *J. Chem. Soc. Chem. Commun.* 114 (1992) 1791-1793, DOI: 10.1039/C39920001791.
24. V. A. Shilin, A. A. Szhogina, M. V. Suyasova, V. P. Sedov, V. T. Lebedev, V. S. Kozlov, Fullerenes and fullereneols survival under irradiation, *Nanosystems: Physics, chemistry, mathematics*, 7 (2016) 146-152, DOI 10.17586/2220-8054-2016-7-1-146-152.
25. I. I. Finegol'd, D. A. Poletayev, R. A. Kotelnikova, A. B. Kornev, P. A. Troshin, I. E. Kareev, V. P. Bubnov, V. S. Romanova, A. I. Kotelnikov, Membranotropic and relaxation properties of water-soluble derivatives of gadolinium endometallofullerenes, *Russian Chemical Bulletin*, 63 (2014) 1107-1112
26. B-C. Wang, H-W. Wang, H-C. Tso, T-L. Chen, Y-M. Chou, Theoretical studies of $\text{C}_{70}(\text{OH})_n$ ($n=14, 16, 18$ and 20) fullerols, *Journal of molecular Structure: THEOCHEM*, 581 (2002) 177-186.
27. E. Barsoukov and J. Ross Macdonald, *Impedance Spectroscopy*, Second Edition, edited by. ISBN 0-471-64749-7 Copyright © 2005 by John Wiley & Sons, Inc. 583 c.
28. O. Gunnarsson, Superconductivity in fullerenes, *Reviews of Modern Physics*, 69 (1997) 575-606.
29. H. Yang, C. Lu, Z. Liu, H. Jin, Y. Che, M. M. Olmstead, A. L. Balch, Detection of a family of gadolinium-containing endohedral fullerenes and the isolation and crystallographic characterization of one member as a metal-carbide encapsulated inside a large fullerene cage, *J. Am. Chem. Soc.* 130 (2008) 17296-17300.
30. N. G. Bukun, A. E. Ukshe, Impedance of solid electrolyte systems, *Russian journal of Electrochemistry* 45 (2009) 11-24, DOI: 10.1134/S1023193509010030.
31. J. C. Dyre, T. B. Schroder, Universality of AC conduction in disordered solids, *Rev. Mod. Phys* 72 (2000) 873-891, 10.1103/RevModPhys.72.873.
32. P. Mondal, P. Lunkenheimer, A. Loidl, Dielectric relaxation, AC and DC conductivities in the fullerenes C_{60} and C_{70} , *Zeitschrift für Physik B Condensed Matter* 99 (1996) 527-533.
33. Edited by Mickaël Lallart, *Ferroelectrics - Physical Effects*. Publisher: InTech, Chapter published. 2011, 666 p., 77-100 pp.
34. K. Hinokuma, M. Ata, Proton conduction in polyhydroxy hydrogensulfated fullerenes, *Journal Electrochemical Society* 150 (2003) A112-A116, DOI:10.1149/1.1527051.
35. J. Li, A. Takeuchi, M. Ozawa, X. Li, K. Saigo, L. Kitazawa, C_{60} fullerol formation catalysed by quaternary ammonium hydroxides, *J. Chem. Soc. Chem. Commun.* (1993) 1784-1786.

Proton conductivity of $\text{Gd@C}_{82}\text{O}_x(\text{OH})_y$ ($x+y=40-42$) is 10^{-10} S/cm

At temperatures below 260 K the residual polarization amount up $3.3 \cdot 10^{-4}$ $\mu\text{C}/\text{cm}^2$

A large number of O and OH groups affect on the amount of residual polarization

Reach-through conductivity suppresses polarization at temperatures above 260 K

ACCEPTED MANUSCRIPT